



W' -like Resonances in the $t\bar{b}$ Decay Channel with 1 fb^{-1}

The CDF Collaboration
URL <http://www-cdf.fnal.gov>
(Dated: March 21, 2007)

We use the tools of the single top analysis to search for resonant $t\bar{b}$ (+c.c) pair production in a sample of approximately 1 fb^{-1} of $p\bar{p}$ collisions at the Fermilab Tevatron. We look for unexpected structure in the spectrum of the invariant mass of the reconstructed W boson and two leading jets (M_{Wjj}). Expected contributions from Standard Model (SM) processes are derived from selections and background studies of the single top analysis. Resonant $t\bar{b}$ production is modeled as a simple W' with SM-like couplings to fermions. We establish expected sensitivity over the W' mass range from $300 \text{ GeV}/c^2$ to $950 \text{ GeV}/c^2$, derive 95% CL upper limits for $\sigma \cdot BR(W' \rightarrow t\bar{b})$ as a function of the W' mass and compare to expectation.

Preliminary Results for Winter 2007 Conferences

I. INTRODUCTION

The recent progress in single top methods at CDF can be applied to search for unexpected new production mechanisms for $t\bar{b}$ (*+c.c.*) at large q^2 . Resonant tb production is often described in terms of massive W -like bosons, generically called W' , that appear in models with left-right symmetry [1], extra dimensions [2], Little Higgs [3], and topcolor [4]. For simplicity, we will refer to our search for a W' -like tb resonance as a search for W' .

We search for events of the form $W' \rightarrow tb \rightarrow Wbb \rightarrow l\nu jj$ (W +jets). The simplest manifestation of a tb resonance would be an unexpected narrow structure in the invariant mass of the reconstructed W and two leading jets (M_{Wjj}) and a Jacobian peak in the transverse momentum of the leading b jet or reconstructed top [5].

CDF studied this distribution in the small Run I sample and excluded a right-handed W' boson with mass less than about 550 GeV/ c^2 [6]. DØ has recently used the W +2 jet channel in 230 pb $^{-1}$ to establish model-dependent limits ruling out W' bosons below the 610-670 GeV/ c^2 range. Here, using the selection and background techniques of the single top analysis, we search for resonant tb states in 1 fb $^{-1}$ of $p\bar{p}$ collisions at $\sqrt{s} = 1.96$ TeV. Modeling the resonance as a simple W' -like boson, we set limits on the production cross-section as a function of the pole mass and effective gauge coupling.

II. DATA SAMPLE & EVENT SELECTION

We use 955 pb $^{-1}$ of CDF Run II data taken through Feb 2006. We employ the same W +jets event selection as the Single-Top group for the 1 fb $^{-1}$ analyses, though we also include the 3-jet channel as part of our signal region. The CDF detector is described in detail in [9].

We require exactly one lepton with large transverse momentum ($P_T \geq 20$ GeV) and isolation from jets, large missing transverse energy ($E_T \geq 25$ GeV), two or three energetic jets ($E_t \geq 15$ GeV and $|\eta_{detector}| < 2.8$), and at least one of the jets must have a displaced secondary vertex (tight SecVTX tag).

In the data we find 644 candidate events with 2 jets and 279 events with 3 jets, consistent with the single top analysis. In order to better validate our model in the side-bands, we will also retain the 1217 events with a single jet, though this channel will not be included in our measurement.

III. BACKGROUNDS

Our backgrounds and their normalizations are listed in Table I. We use the same “Method 2” normalizations and shapes as the single top analysis. All backgrounds other than the non- W (QCD-dominated) component are modeled with ALPGEN + HERWIG and PYTHIA Monte Carlo samples. We model mistagged events using W +light flavor Monte Carlo without a secondary vertex requirement.

Background	2 Jets	3 Jets
Wbb	170.9 ± 50.7	38.2 ± 10.2
$Wc\bar{c}$	63.4 ± 19.9	15.2 ± 4.8
Wcj	68.6 ± 19.0	12.3 ± 3.4
Mistags	136.1 ± 19.7	42.9 ± 7.0
Non- W	26.2 ± 15.9	26.2 ± 15.9
$t\bar{t}$	58.35 ± 13.46	129.03 ± 29.62
Singtop (s+t)	37.8 ± 5.87	8.83 ± 1.37
WW	5.5 ± 0.96	1.69 ± 0.32
WZ	7.96 ± 0.83	2.05 ± 0.28
Z +Jets	11.92 ± 4.42	4.47 ± 2.79
Total BG	587.8 ± 96.5	257.5 ± 39.7
Data	644	279

TABLE I: Number of expected background events in 955 pb $^{-1}$ for 2-jet and 3-jet events.

A. Non- W Model

We want to model the non- W shape by selecting a QCD-enriched sample from the data. We choose electrons-like objects which fail two of the five standard ID requirements but pass all the kinematic cuts. These are treated as electrons, and should provide a good kinematic description of the non- W background. The non- W shape for both central electrons and muons are modeled using this sample. To model electrons at high- η , we also include a sample of jets with high track multiplicity and high electromagnetic to hadronic energy deposition ratio.

B. Background Templates

We collect backgrounds with similar kinematics into a common histogram (template). We have five templates in total: W +bottom, W +charm, mistag/non- W , $t\bar{t}$, and single-top. Table II shows the composition of each of the templates. We compare our full background model to the data in over 40 different control distributions, separately for one, two, and three jets. Examples are shown in Figures 12 through 16.

Template	BG Components
W +bottom	Wbb, WZ, Z +Jets
W +charm	$Wc\bar{c}, Wc, WW$
$t\bar{t}$	$t\bar{t}$
mistag/non- W	mistag and non- W
single top	s+t channel single top

TABLE II: Composition of background templates.

IV. W' SIGNAL MODEL

The Lagrangian describing the W' coupling to fermions can be written as [10]:

$$\mathcal{L} = g\bar{f}_i\gamma_\mu(C_{ij}^R P_R + C_{ij}^L P_L)W'f_j \sim \bar{f}_i\gamma_\mu(g_R \exp^{i\omega} \cos\zeta V_{f_i f_j}^R P^R + g_L \sin\zeta V_{f_i f_j}^L P^L)W'f_j \quad (1)$$

where $P_{L,R} = (1 \pm \gamma_5)/2$ are the projection operators, g is the gauge coupling, and the $C_{ij}^{L,R}$ are arbitrary coupling that differ for quarks and leptons. Figure 1 shows the dominant s-channel diagram for W' production. Contributions from the t - and u - channels are suppressed by the large W' mass.

In models where the W and the W' mix, the mixing angle ζ is typically very well constrained, so the search for a W' can be restricted to purely L or R-handed states. In this case, $\zeta = 0$ and the Lagrangians for the right and left-handed W' coupling to fermions are: $\mathcal{L}_R = \bar{f}_i\gamma_\mu g_R V_{f_i f_j}^R W'f_j$ and $\mathcal{L}_L = \bar{f}_i\gamma_\mu g_L V_{f_i f_j}^L W'f_j$. Furthermore, to make definite numerical predictions, Ref. [10] assumes that $V_{\ell\nu}^R = V_{\ell\nu}^L = \mathbf{I}$ is the identity matrix, while $V_{qq'}^R = V_{qq'}^L = V_{CKM}$ is the Cabibbo-Kobayashi-Maskawa (CKM) matrix with $|V_{tb}| = 1$.

There are two differences between the R-handed and the L-handed W' models:

- ★ The L-handed W' bosons are expected to interfere with the standard model $W \rightarrow t\bar{b}$ process, also known as s -channel single-top production. A discussion of this interference is given later in the text. The R-handed W' bosons do not interfere with the s -channel single-top due to the different final states.
- ★ In regard to R-handed W' models only, we distinguish two cases depending on the mass of the R-handed neutrinos:
 - a. If $M_{\nu_R} > M_{W'}$ then the R-handed and L-handed $W' \rightarrow t\bar{b}$ processes have the same cross-section (modulo the interference point mentioned above)
 - b. If $M_{\nu_R} < M_{W'}$ then the R-handed and L-handed $W' \rightarrow t\bar{b}$ processes have different cross-sections, as the R-handed W' has more decay channels open. This will lead to a lower $W'_R \rightarrow t\bar{b}$ cross-section than that of $W'_L \rightarrow t\bar{b}$.

In Ref. [10], the W'_L width and cross-sections are calculated neglecting the effect of the Standard Model $W \rightarrow t\bar{b}$ process. Following the lead of Ref. [10], we also neglect the interference between the L-handed W' and the s -channel single-top. For clarity, we remind the reader that both of these processes are included in the search, W' as signal, and s -channel single-top as part of the background. It is the interference term that is not included, which is a good approximation especially for the high-mass region: $M_{W'_L} \gg M_W$ [11]. The effect of interference would be to slightly alter the high tail of s -channel single-top and the low tail of the W'_L process.

If the W/W' interference is neglected, then as far as our analysis results are concerned the W'_L models are identical with the W'_R models if $M_{\nu_R} > M_{W'}$. The Monte Carlo program we used to model both W'_L and W'_R was Pythia $p\bar{p} \rightarrow W' \rightarrow t\bar{b}$, where handedness is irrelevant since no W/W' interference is assumed. The only separation of models appears for the R-handed W' bosons if we do or do not allow extra decays to R-handed leptons – cases **a.** and **b.** above – and comes in only through the different $W'_R \rightarrow t\bar{b}$ branching fraction. In other words, all distributions are the same, but the **a.** and **b.** normalizations are different.

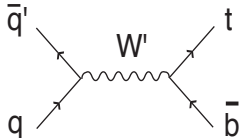


FIG. 1: Representative Feynman diagram for W' production.

We model resonant $t\bar{b}$ production with a heavy, charged boson (W') with the same fermion couplings as the W . We assume a model without interference with the SM W boson and associated single top production. Our W' is thus a good approximation of any new state appearing as, or approximated by, a Lorentzian enhancement in a narrow region of the $M_{t\bar{b}}$ spectrum. We generated PYTHIA Monte Carlo (MC) samples for W' masses from 300 GeV/ c^2 to 950 GeV/ c^2 in 50 GeV/ c^2 increments.

V. CALCULATION OF EXPECTED LIMITS IN M_{Wjj}

We search the M_{Wjj} distribution for evidence of W' production by creating ensembles of pseudo experiments (PE's). We compare the agreement of two hypotheses with Poisson-fluctuated data (pseudo data) using the program MCLIMIT.

The null hypothesis, H_B , asserts that the pseudo data are fully described by the standard model as characterized by our background model. The signal + background hypothesis, H_{S+B} , asserts that the pseudo data are comprised of the SM background plus some fraction W' events. We define a test statistic to quantify the agreement between the pseudo-data and our hypotheses for a specified signal fraction.

A. Frequentist Test Statistic

We set modified frequentist limits by measuring the agreement of the hypotheses with the data using the ratio of their likelihood values,

$$Q = \frac{\chi^2(\text{data}|H_{S+B})}{\chi^2(\text{data}|H_B)}, \quad (2)$$

Likelihood minimization is performed using MINUIT. Taking the logarithm, we can define $\Delta\chi^2$.

$$-2 \ln Q = \chi^2(\text{data}|H_{S+B}) - \chi^2(\text{data}|H_B) \equiv \Delta\chi^2 \quad (3)$$

Our variable of merit combines the probability of each of the two hypotheses and is defined by

$$CL_S = \frac{P_{S+B}(\Delta\chi^2 \geq \Delta\chi^2_{\text{obsv}})}{P_B(\Delta\chi^2 \geq \Delta\chi^2_{\text{obsv}})} \quad (4)$$

B. Calculating Upper Limit

We account for the rate and shape uncertainties by assigning a corresponding “nuisance parameters” whose value varies from PE to PE and is drawn from a Gaussian of mean X and standard deviation Y . The mean is specified by the nominal value of the systematic uncertainty, and the width is set by its uncertainty. Thus all systematic uncertainties are modeled internally and their effect is automatically incorporated into the final result.

We construct ensembles of 15k PE’s and vary the signal fraction in the H_{S+B} hypothesis. Our expected limits are determined by finding the amount of signal needed in order for 95% of the H_{S+B} Q-values to be larger than the median Q for H_B . We can similarly calculate the $\pm 1\sigma$ deviations from the expected limit by finding the amount of signal needed for 95% of the H_{S+B} Q-values to be larger than the $\pm 1\sigma$ Q for H_B . The observed limit is set when 95% of the Q-values larger than Q for the data come from H_{S+B} , i.e. $CL_S \leq 0.05$.

C. Combining 2 and 3-Jet Channels

The M_{Wjj} distribution in 2 and 3 jets can be combined for enhanced signal sensitivity. This procedure calculates the total test statistic by using the same nuisance parameters for 2 and 3 jets in each summing the χ^2 across the bins in both channels: $\Delta\chi_{total}^2 = \Delta\chi_{2-jet}^2 + \Delta\chi_{3-jet}^2$.

Figure 3 compares the combined expected limits with those obtained by treating the channels separately. Clearly the combined sensitivity is dominated by the 2 jet channel.

VI. SYSTEMATIC UNCERTAINTIES

Our full systematic uncertainty includes contributions from uncertainty in the template normalizations, jet energy scale (JES), initial state radiation (ISR), final state radiation (FSR), the ALPGEN Monte Carlo Factorization/Renormalization (Q^2) scale, mistag shape, non-W shape, parton distribution functions (PDF), and luminosity. First, we discuss the treatment of rate and shape systematic uncertainties in our pseudo experiments. Then we discuss our method for estimating each systematic uncertainty.

A. Systematic Uncertainties in Pseudo Experiments

We incorporate normalization uncertainties by assigning a corresponding nuisance parameter in our PE’s. These parameters are independently varied within a Gaussian constraint during each PE. Thus the mean of the Gaussian fluctuation for a particular nuisance parameter is the nominal expected normalization, and the width is set by the uncertainty on that normalization.

Shape uncertainties are also treated by assigning them a nuisance parameter which can vary within a Gaussian constraint. The value of the nuisance parameter for a particular PE corresponds to the amount by which we shift our template for that PE. This is often referred to as template morphing. All template morphing is performed by PVMORPH, using a horizontal interpolation algorithm.

To generate each shifted template, our PE code uses the unshifted original shape and the $\pm N\sigma$ (N may differ for various systematic uncertainties) shifted shapes to interpolate any amount of shape variation within the bounds of $\pm N\sigma$. Because extrapolation beyond this range is less certain, we truncate the nuisance parameter for the shape variation at $\pm N\sigma$. Thus \pm templates input into the code set the bounds in which we can vary the template morphing.

We include all shape variations simultaneously in our expected limit calculations. MCLimit calculates the shape variation for each parameter independently during a PE, then averages all the shifted templates for the overall shift. We acknowledge that this procedure neglects the correlations (or anti-correlations) between sources of systematic uncertainty. We anticipate the overall impact of correlations is small among our major systematic uncertainties and we do not attempt a more sophisticated treatment at this time.

B. Estimation of Each Systematic Uncertainty

Background Normalization: The overall normalization uncertainty, including acceptance systematic uncertainties of 0.5% for lepton ID and 8% for the b -tag scale factor correction, is shown for background components in Table I.

Signal Acceptance: The signal acceptance includes uncertainty from several sources. Lepton ID represents is a 0.5% source of uncertainty. Dataset luminosity for our sample is uncertain to within 6% ($954.7 \pm 57.28 \text{ pb}^{-1}$)

B-tag scale factor: The b-tag scale factor uncertainty is our dominant systematic uncertainty. We use the central value of 0.89 for the b-tag scale factor. The uncertainty for $t\bar{t}$ -like b-tagged jet E_T is 8%. Jets from decay of a massive W' have a much larger E_T than jets from a typical $t\bar{t}$ event. There are very few high- E_T tagged jets in the data and scale factor is not precisely measured for such jets. The highest E_T jets we observed in data have a statistical uncertainty of 17%. Thus we use this value as the uncertainty for all our signal samples. **Jet Energy Scale (JES):** We generate the $\pm 1\sigma$ JES shifted shapes for our signal and MC backgrounds by adding all sources of jet uncertainty in quadrature. We use PVMORPH to extrapolate the $\pm 1\sigma$ shapes shifts (including normalization changes) out to $\pm 3\sigma$. We use the 3σ varied templates to vary the JES within these bounds during the PE's.

Initial/Final State Radiation (ISR/FSR): We generated monte carlo samples with more/less radiation for signal samples with $M(W') = 300, 500, 700, 900 \text{ GeV}/c^2$. We then interpolate for all the intermediate masses. These templates are treated as 1σ bounds, thus we vary ISR/FSR within this range during our PE's.

ALPGEN Factorization/Renormalization scale (Q^2): W+jets Monte Carlo is produced using ALPGEN. The choice of factorization/renormalization scale (Q^2) impacts the shape of those W+jets MC samples. To estimate the uncertainty arising from the Q^2 scale, we created alternate shape templates for heavy-flavor ($Wb\bar{b}, Wc\bar{c}, Wc$) backgrounds in generated with an alternate $Q^2 = M_W^2$. We consider only the variations in shape. We include these alternate shape templates as 1σ variations in our pseudo experiments. Although the W+light flavor MC used for our mistag model is also affected by Q^2 , the mistag shape uncertainty (discussed below) subsumes any Q^2 dependence.

Mistag Model: We estimate the uncertainty in using pretag MC to model the mistag shape by comparing to an alternative template made from pretag data as a 1σ shape variation when performing our PE's.

Non-W Model: Due to the small non-W fraction remaining after our QCD cuts, we do not expect to be sensitive to changes in the non-W shape. Nonetheless, we estimate our shape uncertainty by treating our mistag shape as a 1σ shape variation when performing our PE's.

Parton Distribution Function (PDF): We estimated the impact of using different parton distribution functions using event reweighting. Reweighting involves calculating a new weight for each event based on x_1 and x_2 , the incoming parton momenta, and Q^2 , the momentum transfer. The incoming parton momenta are process-independent. For W' production, $Q^2 = \hat{s} = M(W')^2$.

The resulting systematic uncertainty ranged from 1.5% to 3.9%, depending upon mass. For our pseudo experiments, we conservatively use a 4% overall PDF uncertainty for all masses.

VII. FINAL RESULTS

A. Limits on W' Mass

Figure 4 shows our final result in 2+3 jets. The observed limit has fluctuated low to near the -1σ expected limit in the high-mass range.

Figure 5 shows the observed limit plotted with the theoretical prediction [10]. We exclude at 95% confidence level models whose theoretical cross-section exceeds the observed limit. Based on a linear extrapolation from 850 to 900 GeV/c^2 and rounding down to the nearest 10 GeV/c^2 , we exclude with 95% confidence models with $M(W') > M(\nu_R)$, $M(W') < 760 \text{ GeV}/c^2$ and with $M(W') < M(\nu_R)$, $M(W') < 790 \text{ GeV}/c^2$.

1. Deviation from Expected Limit

Figures 6 and 7 show the the observed limit in the 2-jet bin and 3-jet bin exclusively. The 2-jet bin dominates the behavior of the combined limit.

There is a slight excess over expectation observed in the region near 450-500 GeV/c^2 . Figure 6 shows this contribution arises from the 2-jet bin. Figures 8 and 9 show further that this excess arises in the electron sample.

Figure 11 shows the mass distribution in the data. The 2-jet bin at approximately $475 \text{ GeV}/c^2$ shows an excess. The bin's width ($20 \text{ GeV}/c^2$) is on the order of our top mass resolution. Since the predictions in the neighboring bins agree with the observation, and since the three jet bin does not show a similar excess, we anticipate that the excess in this region is a statistical fluctuation.

Figure 4 shows the observed limit is close to the -1σ fluctuation for $M(W') > 600 \text{ GeV}/c^2$. We expect such a fluctuation in approx. 16% of all pseudo experiments. At first it seems unlikely that such a fluctuation would persist across many different W' masses. For instance, the fluctuation from the bin spanning $460\text{-}480 \text{ GeV}/c^2$ only strongly impacts the limits at masses of 450 and 500 GeV/c^2 . However, looking at figure 11 shows that the -1σ fluctuation persists for $M(W') > 600$ because all of those masses are looking for signal events in the overflow bin. Our MC only provides enough statistics to estimate the backgrounds out to $660 \text{ GeV}/c^2$. Events with mass larger than $660 \text{ GeV}/c^2$ are placed in the $640\text{-}660 \text{ GeV}/c^2$ bin. Limits on masses larger than $660 \text{ GeV}/c^2$ are putting limits on the content of that final bin. Any limit will be constrained by the statistics of the $640\text{-}660 \text{ GeV}/c^2$ bin.

B. Limits on W' Coupling Strength

The last part of our discussion regards setting limits in the $M_{W'} - g$ plane. As seen in the beginning of this section, the gauge coupling $g_{R,L}$ comes in as a multiplicative parameter in the Lagrangian. Given that there are two $qW'q$ vertices in the leading order diagram of Fig. 1, the total $p\bar{p} \rightarrow W' \rightarrow t\bar{b}$ cross-section will be proportional to g^4 , where g denotes either the g_R or the g_L coupling depending on the model we are testing. So far we have assumed $g = g_{SM}$. However, this does not have to be the case, and we can test models with different values of g . In fact, if we assume that the width of the reconstructed W' mass distribution is dominated by detector effects (see CDF 8597) then a model with $g \neq g_{SM}$ would have an identical reconstructed W' mass distribution as a $g = g_{SM}$ model, but a normalization which differs by a factor of g^4/g_{SM}^4 . For a given mass $M_{W'}$ we can adjust g until the cross-section of the model calculated via scaling by g^4/g_{SM}^4 equals the experimentally excluded cross-section. This is precisely how the $M_{W'} - g$ graph shown in Figure 10 is constructed. As seen in this plot, we exclude gauge couplings down to $0.45g_{SM}$ for low W' masses and $M(W') < M(\nu)$.

VIII. CONCLUSION

We use 955 pb^{-1} of CDF Run II data and find no evidence for resonant W' production. We exclude a W' with SM couplings which decays via $W' \rightarrow t\bar{b}$ for $M(W') < 760 \text{ GeV}/c^2$ in the case of $M(W') > M(\nu_R)$, and we exclude $M(W') < 790 \text{ GeV}/c^2$ in the case of $M(W') < M(\nu_R)$. Constraints on the coupling to fermions are shown in Fig. 10.

Acknowledgments

We thank the Fermilab staff and the technical staffs of the participating institutions for their vital contributions. This work was supported by the U.S. Department of Energy and National Science Foundation; the Italian Istituto Nazionale di Fisica Nucleare; the Ministry of Education, Culture, Sports, Science and Technology of Japan; the Natural Sciences and Engineering Research Council of Canada; the National Science Council of the Republic of China; the Swiss National Science Foundation; the A.P. Sloan Foundation; the Bundesministerium fuer Bildung und Forschung, Germany; the Korean Science and Engineering Foundation and the Korean Research Foundation; the Particle Physics and Astronomy Research Council and the Royal Society, UK; the Russian Foundation for Basic Research; the Comision Interministerial de Ciencia y Tecnologia, Spain; and in part by the European Community's Human Potential Programme under contract HPRN-CT-20002, Probe for New Physics.

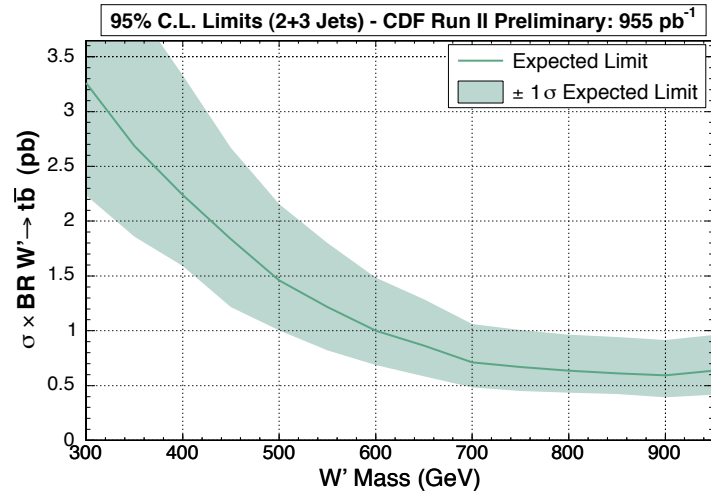


FIG. 2: Expected limits in the 2+3 jets for 5k pseudo experiments.

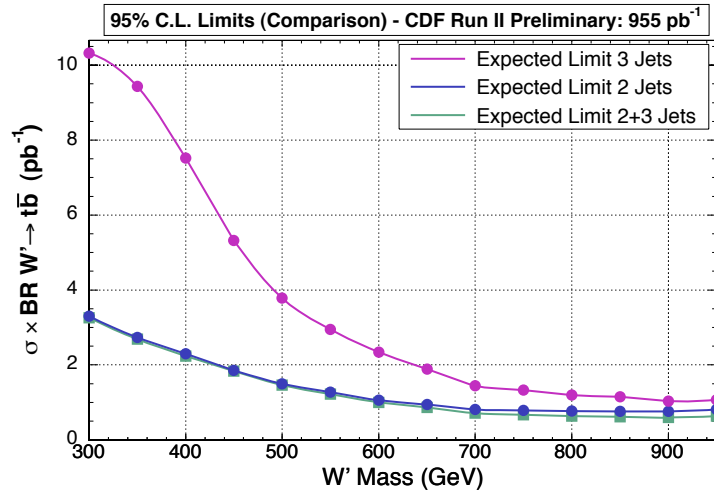


FIG. 3: Direct comparison of limits in 2-jets, 3-jets, and 2+3 jets.

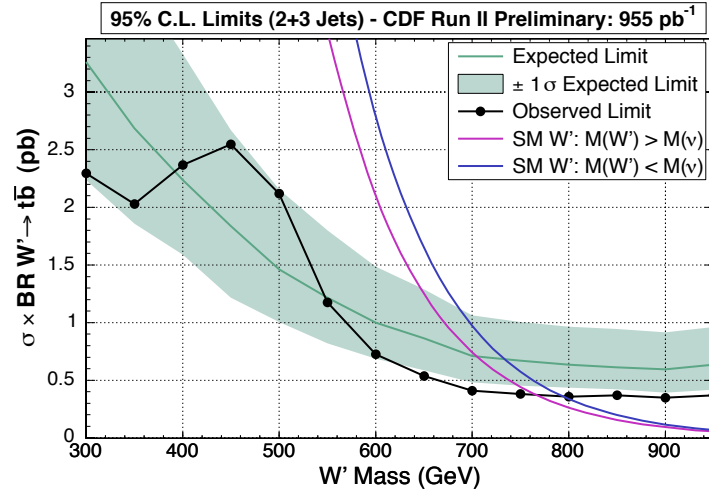


FIG. 4: Observed limits in the 2+3 jets.

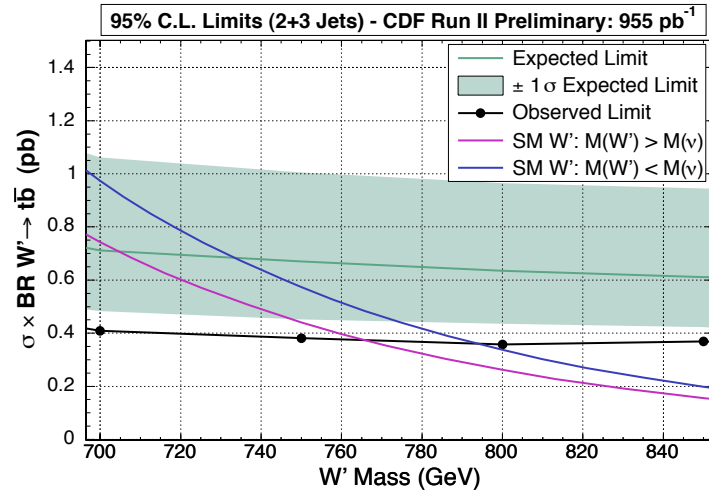


FIG. 5: Observed limits in the 2+3 jets, enlarged to show the high mass region.

-
- [1] J.C. Pati, A. Salam, Phys. Rev.**D10**, 275 (1974)
R. Mohapatra and J. Pati, Phys. Rev.**D11**, 566 (1975).
- [2] Y. Mimura, S. Nandi, Phys. Lett. **B538**, 406 (2002)
G. Burdman, B. Dobrescu, E. Ponton, Phys.Rev.**D74** (2006) 075008.
- [3] see e.g. M. Perelstein, hep-ph/0512128 and Prog.Part.Nucl.Phys. 58 (2007) 247-291.
- [4] E. Malkawi, T. Tait, C.P. Yuan, Phys. Lett.**B385**, 304 (1996)
H. Georgi, E. Jenkins, E. Simmons, Nucl. Phys**B331**, 541 (1990).
- [5] Still looking for this...
- [6] H. Kim, P. Savard, P. Sinervo, S. Truitt "Search for $W' \rightarrow tb$ Using $bbl\nu$ Final States" CDFNote 5000, May, 1999, published in Phys. Rev. Lett. **90**, 081802 (2003).
- [7] The D0 Collaboration, Phys. Lett. **B641**
- [8] $W' \rightarrow l\nu_l$ at CDF: The CDF Collaboration, Phys. Rev. Lett. 67, 2609 (1991).
The CDF Collaboration, Phys. Rev. Lett. 74, 2900 (1995).

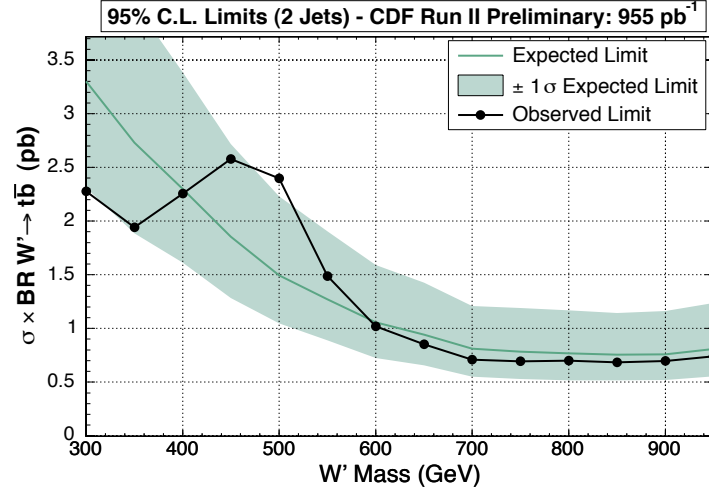


FIG. 6: Observed limits and expect limits in the 2-jet bin.

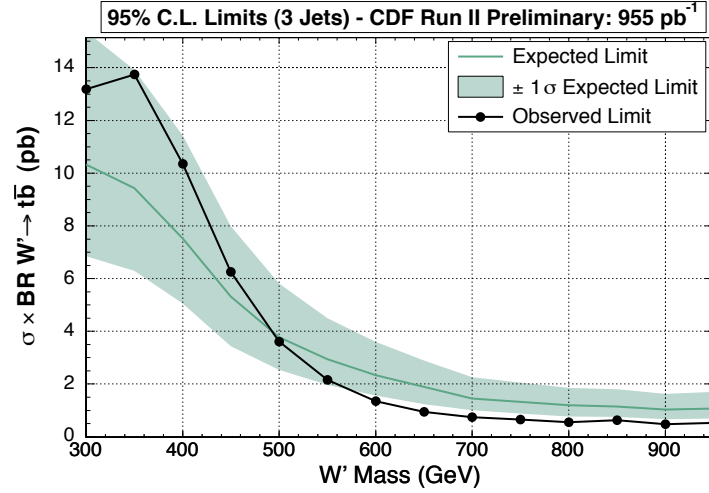


FIG. 7: Observed limits and expected limits in the 3-jet bin.

The CDF Collaboration, Phys. Rev. Lett. 84, 5716 (2000).

The CDF Collaboration, FERMILAB-PUB-06-419-E. Submitted to Phys. Rev. D Rapid Communications November 9, 2006.

$W' \rightarrow t\bar{b}$ at CDF: The CDF Collaboration, Phys. Rev. Lett. 90, 081802 (2003).

$W' \rightarrow \ell\nu_\ell$ at DØ: The DØ Collaboration, Phys. Rev. Letters 76, 3271 (1996). The DØ Collaboration, Phys. Letters B358, 405 (1995).

$W' \rightarrow t\bar{b}$ at DØ: The DØ Collaboration, Phys. Letters B 641, 423 (2006).

- [9] F. Abe, et al., Nucl. Instrum. Methods Phys. Res. A **271**, 387 (1988); D. Amidei, et al., Nucl. Instrum. Methods Phys. Res. A **350**, 73 (1994); F. Abe, et al., Phys. Rev. D **52**, 4784 (1995); P. Azzi, et al., Nucl. Instrum. Methods Phys. Res. A **360**, 137 (1995); The CDFII Detector Technical Design Report, Fermilab-Pub-96/390-E
- [10] Z. Sullivan, *Fully differential W' production and decay at next-to-leading order in QCD*, Phys.Rev. D66 (2002) 075011, hep-ph/0207290
- [11] Our search region is $M_{W'} > 300 \text{ GeV}/c^2$, and we exclude masses up to approximately $900 \text{ GeV}/c^2$ if SM couplings of the W' to fermions are assumed.

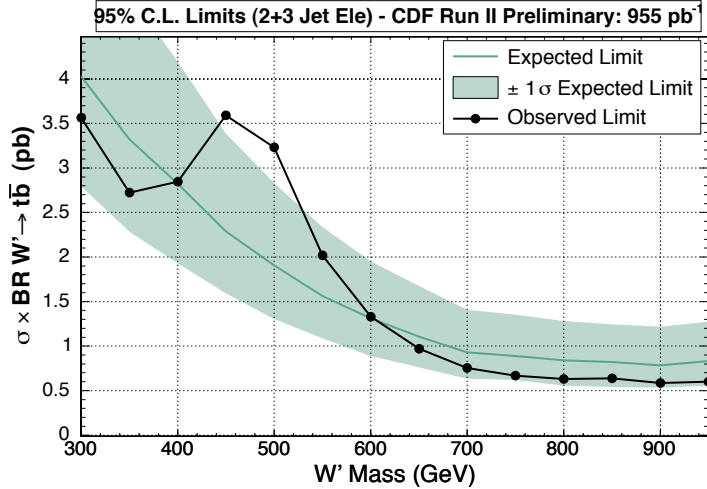


FIG. 8: Observed limits and expected limits in 2+3 jets for electrons.

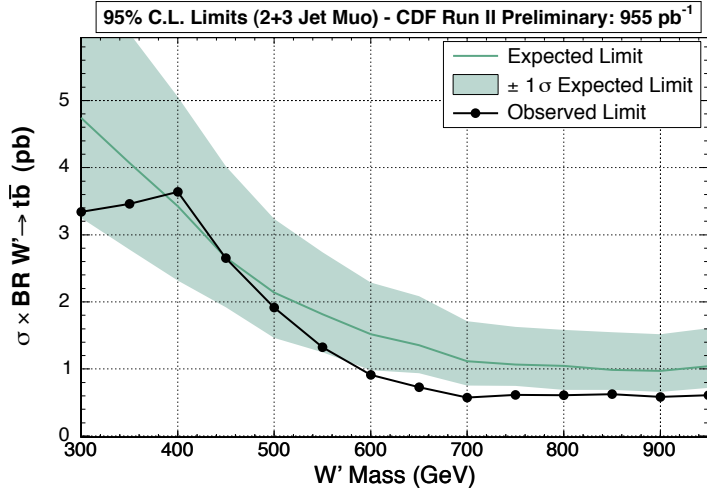


FIG. 9: Observed limits and expected limits in 2+3 jets for muons.

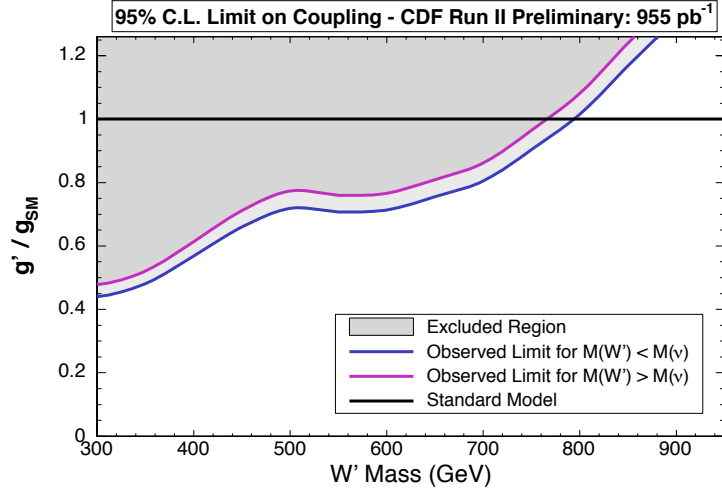


FIG. 10: Observed limits on the ratio of coupling constants, g'/g . We exclude coupling constants in the shaded region with 95% confidence.

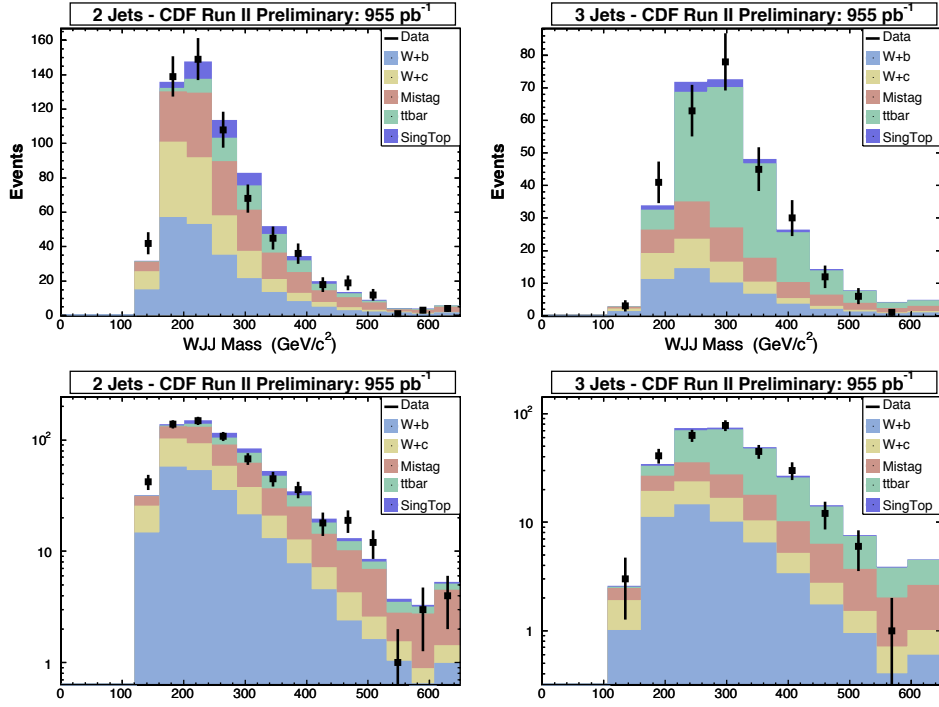


FIG. 11: Background model compared to the data for $M(W')$ in the 2-jet bin and 3-jet bin. The background model has been scaled up by 10% for visual comparison.

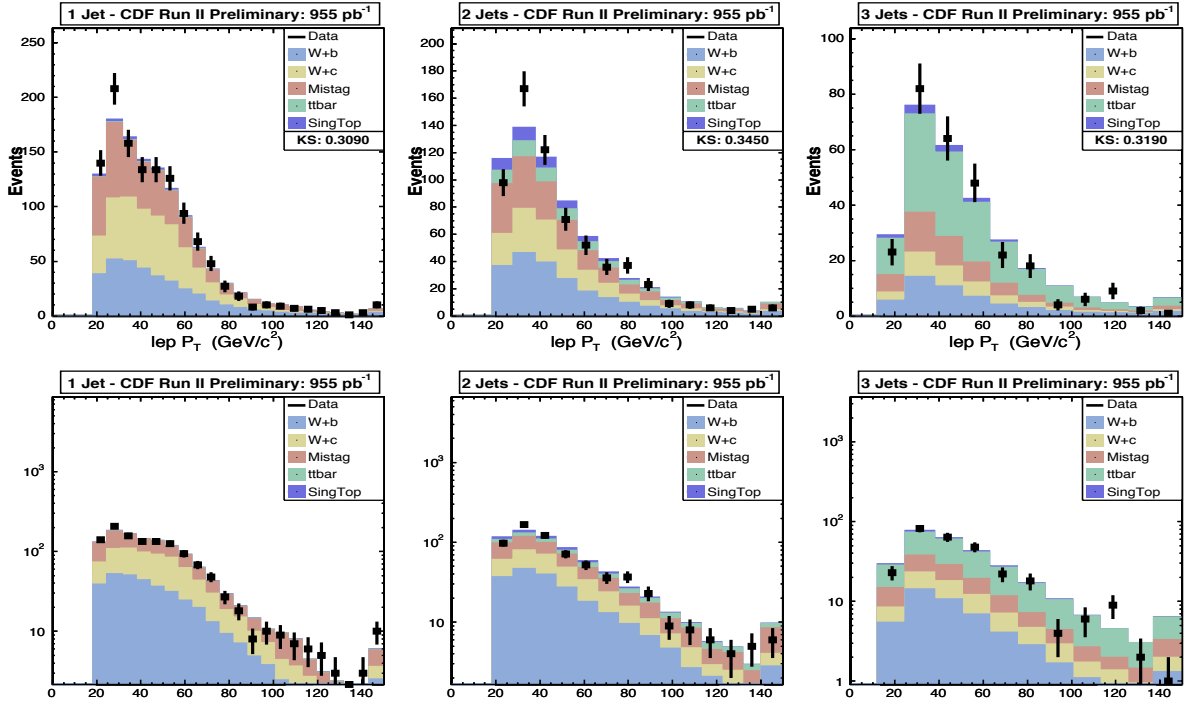


FIG. 12: Comparison of background model to the data. The background model has been scaled up by 10% for visual comparison.

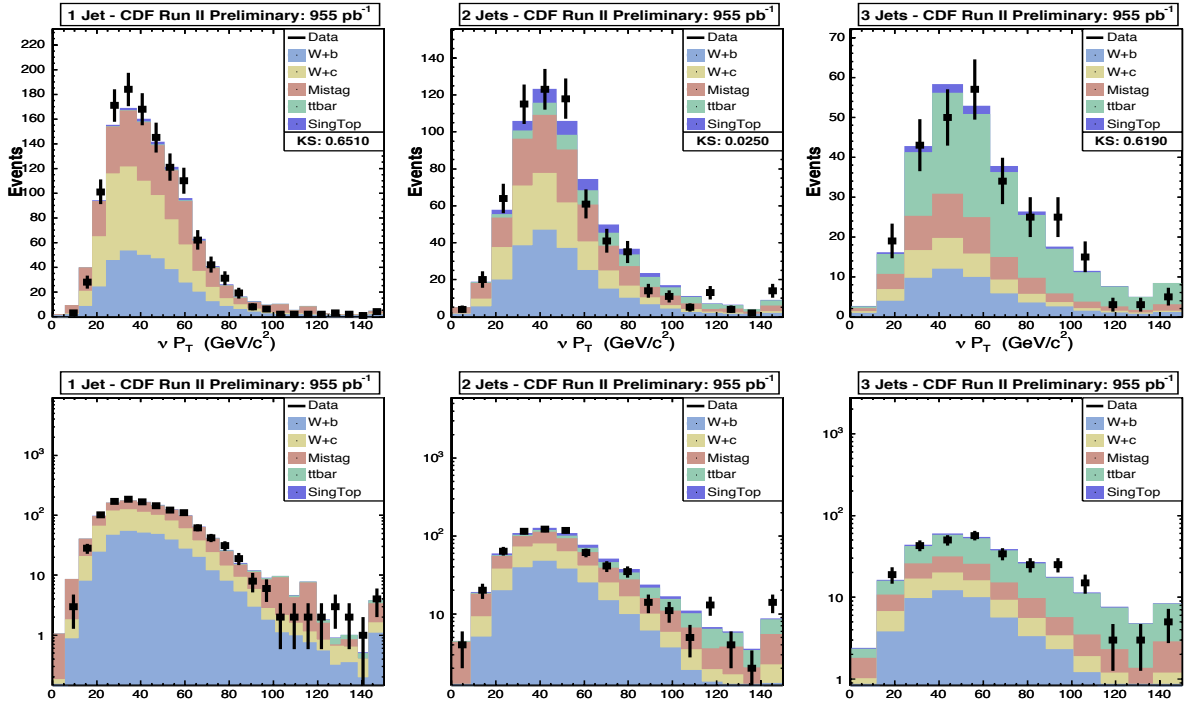


FIG. 13: Comparison of background model to the data. The background model has been scaled up by 10% for visual comparison.

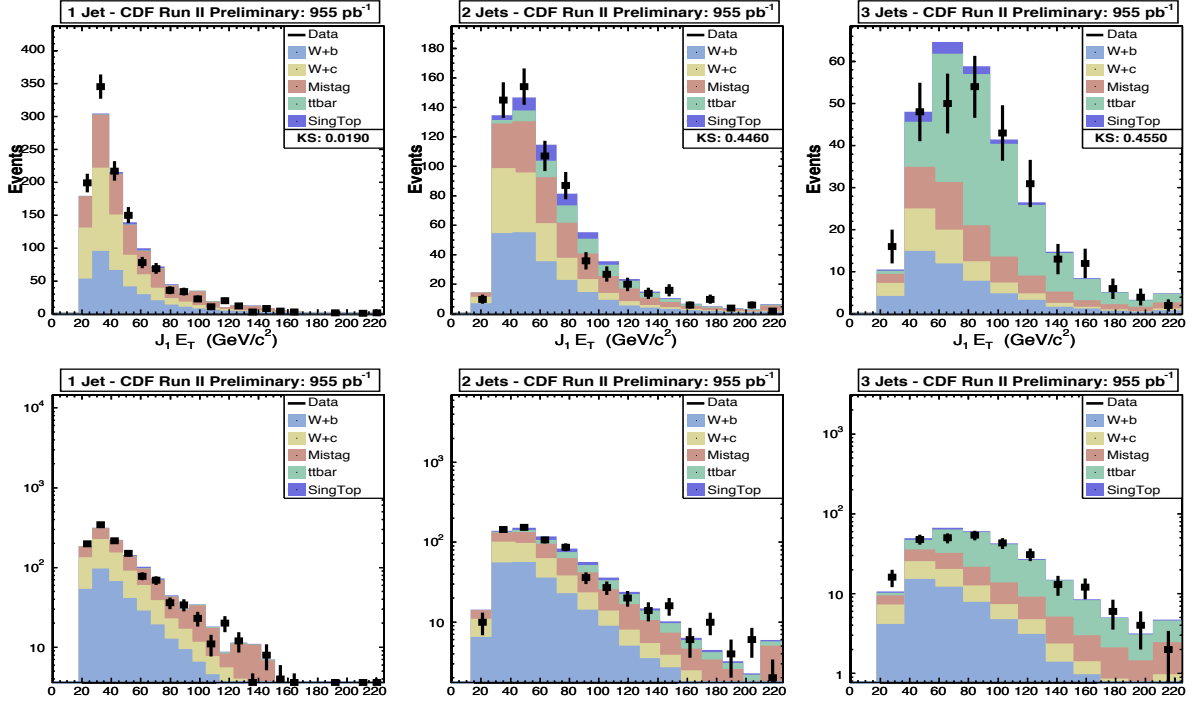


FIG. 14: Comparison of background model to the data. The background model has been scaled up by 10% for visual comparison.

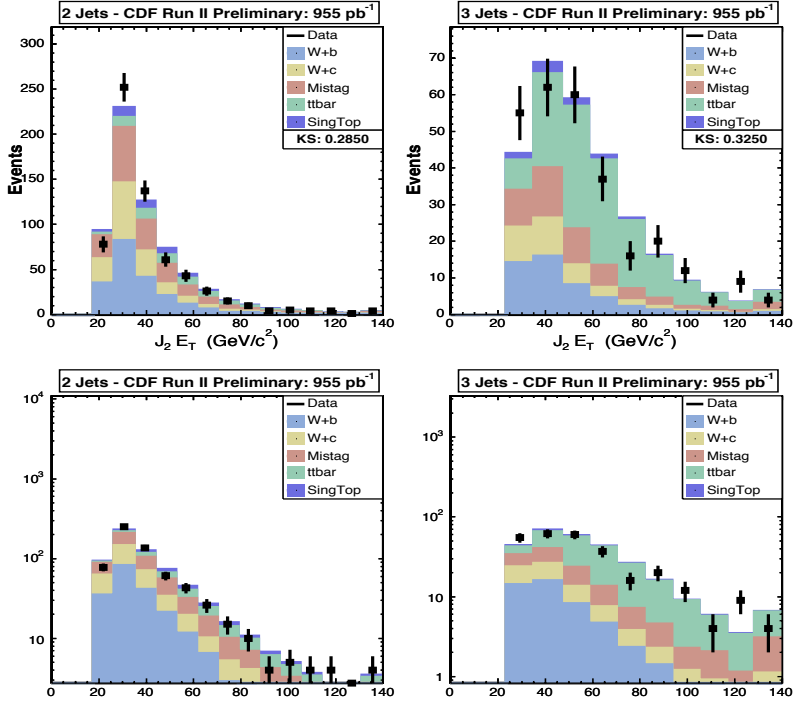


FIG. 15: Comparison of background model to the data. The background model has been scaled up by 10% for visual comparison.

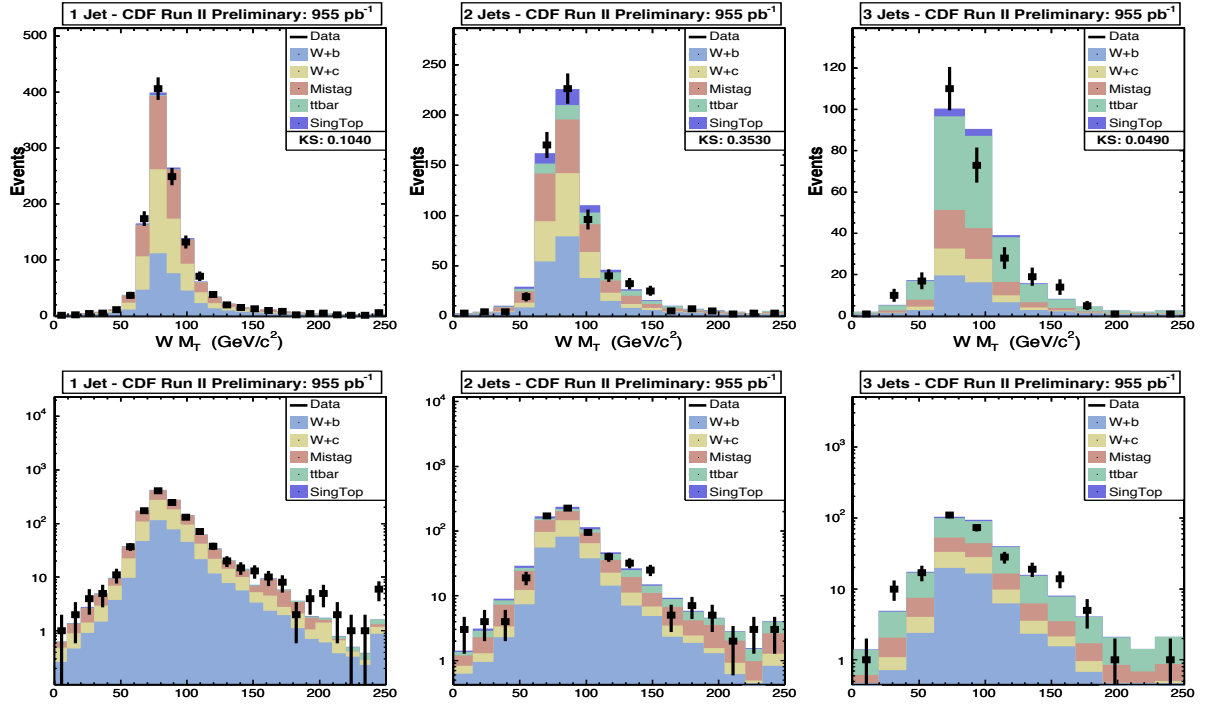


FIG. 16: Comparison of background model to the data. The background model has been scaled up by 10% for visual comparison.